Central Washington University

ScholarWorks@CWU

All Faculty Scholarship for the College of the Sciences

College of the Sciences

4-1-2016

GPS constraints on interplate locking within the Makran subduction zone

Elyse Frohling
Central Washington University

Walter Szeliga
Central Washington University

Follow this and additional works at: https://digitalcommons.cwu.edu/cotsfac

Part of the Geology Commons, Geomorphology Commons, Geophysics and Seismology Commons, and the Tectonics and Structure Commons

Recommended Citation

E. Frohling, W. Szeliga, GPS constraints on interplate locking within the Makran subduction zone, Geophysical Journal International, Volume 205, Issue 1, 1 April 2016, Pages 67–76, https://doi.org/10.1093/gji/ggw001

This Article is brought to you for free and open access by the College of the Sciences at ScholarWorks@CWU. It has been accepted for inclusion in All Faculty Scholarship for the College of the Sciences by an authorized administrator of ScholarWorks@CWU. For more information, please contact scholarworks@cwu.edu.

Geophysical Journal International

Geophys. J. Int. (2016) **205,** 67–76
GJI Geodynamics and tectonics

doi: 10.1093/gji/ggw001

GPS constraints on interplate locking within the Makran subduction zone

E. Frohling and W. Szeliga

Department of Geological Sciences, Central Washington University, Ellensburg, WA 98926, *USA. E-mail:* walter@geology.cwu.edu

Accepted 2016 January 4. Received 2016 January 1; in original form 2015 September 2

SUMMARY

The Makran subduction zone is one of the last convergent margins to be investigated using space-based geodesy. While there is a lack of historical and modern instrumentation in the region, a sparse sampling of continuous and campaign measurements over the past decade has allowed us to make the first estimates of convergence rates. We combine GPS measurements from 20 stations located in Iran, Pakistan and Oman along with hypocentral locations from the International Seismological Centre to create a preliminary 3-D estimate of the geometry of the megathrust, along with a preliminary fault-coupling model for the Makran subduction zone. Using a convergence rate which is strongly constrained by measurements from the incoming Arabia plate along with the backslip method of Savage, we find the Makran subduction zone appears to be locked to a depth of at least 38 km and accumulating strain.We also find evidence for a segmentation of plate coupling, with a 300 km long section of reduced plate coupling. The range of acceptable locking depths from our modelling and the 900 km along-strike length for the megathrust, makes the Makran subduction zone capable of earthquakes up to $M_w = 8.8$. In addition, we find evidence for slow-slip-like transient deformation events on two GPS stations. These observations are suggestive of transient deformation events observed in Cascadia, Japan and elsewhere.

Key words: Space geodetic surveys; Transient deformation; Subduction zone processes; Continental margins: convergent.

1 INTRODUCTION

1.1 Background

The Makran subduction zone stretches approximately 900 km E-W along the southern coasts of Pakistan and Iran and accommodates convergence of the Arabian plate beneath the Eurasian plate at a rate of about 4 cm yr^{-1} over the past 3 Myr (DeMets *et al.* 1990; Kopp *et al.* 2000; Smith *et al.* 2012; Fig. 1). Due to a historical dearth of both local instrumentation and detailed study, the seismic hazards associated with the Makran remain largely unconstrained into the present day. Regional hypocentral studies from global seismic data suggest the eastern part of the subduction zone is more seismically active than the western segment (Byrne *et al.* 1992; Rajendran *et al.* 2013), a suggestion punctuated by the occurrence of a M_w 8.1 earthquake and tsunami in 1945 along the eastern segment (Rajendran *et al.* 2013). However, the lack of local seismic network data and scant crustal deformation measurements have largely precluded the determination of the general nature of plate coupling, and in particular, constraining the occurrence and extent of segmentation along this boundary. Deployment of continuous and campaign GPS over the last decade, coupled with global seismic data, now permit geophysical modelling of plate coupling and strain accumulation rate within the Makran subduction zone.

Since no models of the subduction interface are available for the Makran, we construct a suite of three fault models in an attempt to place bounds on the location of the plate interface. Our suite of fault models include a simple shallowly dipping plane, one constructed from hypocentral data and published moment tensors for regional earthquakes, and one extrapolated from cross-sections published in Byrne *et al.* (1992). These fault models are then combined with assumptions about the plate coupling and used to forward model the velocity field in a Eurasia-fixed reference frame. We then compare the results of our forward modelling with our processed GPS observation data to infer the plate coupling profile for the subduction zone.

In addition to modelling plate coupling, we also note that time-series from two continuous GPS stations in the western Makran show evidence for transient deformation similar to slow-slip events recorded in other subduction zones worldwide (Douglas *et al.* 2005; Gomberg & Cascadia 2007 and Beyond Working Group 2010; Obara 2011). Although we lack station density to conclusively demonstrate these events to be unequivocally slow-slip events, they

© The Authors 2016. Published by Oxford University Press on behalf of The Royal Astronomical Society.

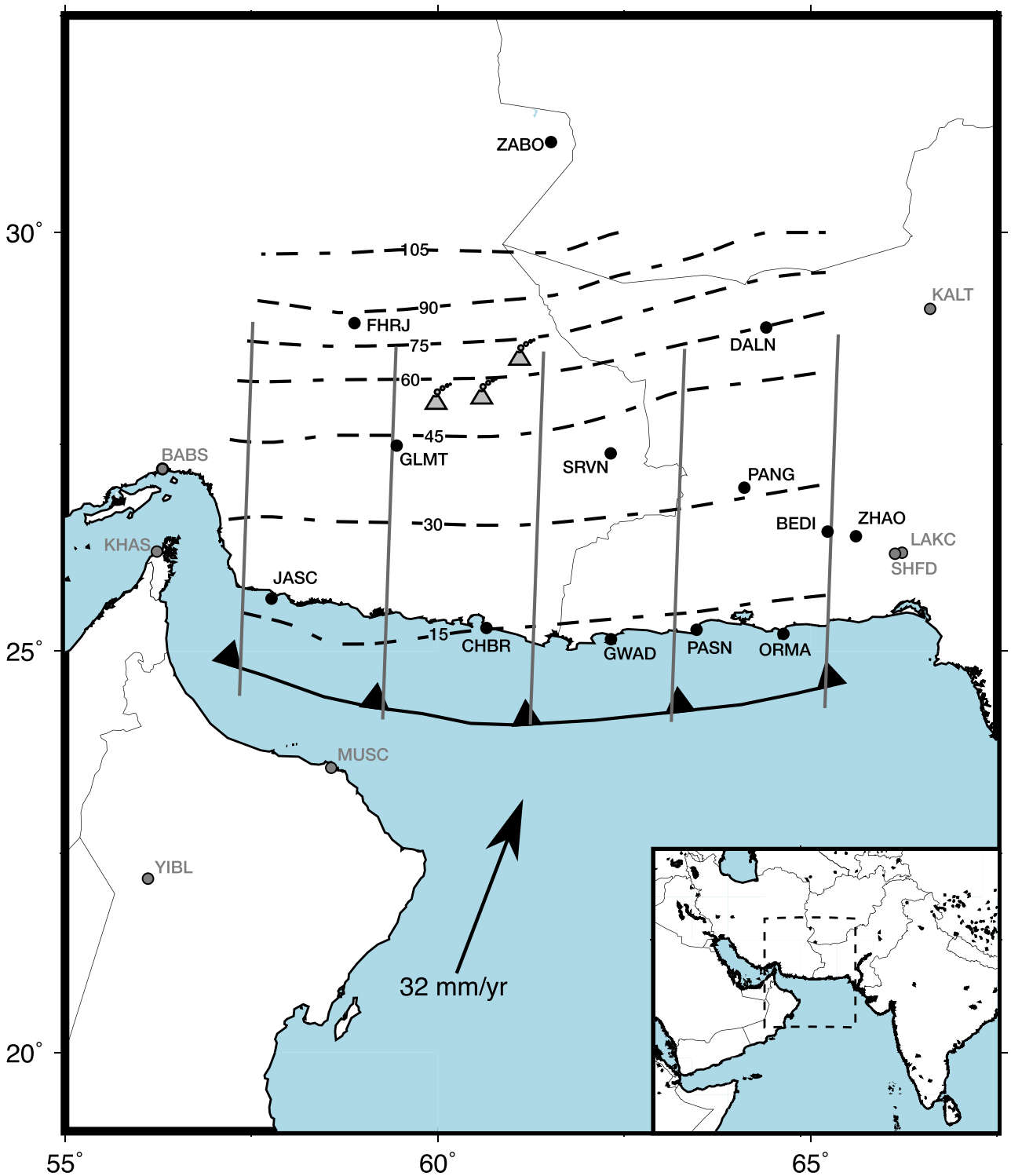

Figure 1. Map showing the location of the Makran subduction zone. GPS stations' names and locations are indicated by filled circles, black circles denote stations used for forward modelling and grey circles denote stations used to delineate the behaviour of adjacent plates. Plate interface contours from the shallow model are shown as dashed lines with a 15 km contour interval. Solid grey lines denote seismic profile locations used in the generation of the plate interface models. Arrow indicates the velocity of the Arabian plate relative to stable Eurasia.

display many of the characteristics observed in other subduction zones, such as their location, just trench-ward of the volcanic arc, week-long duration, reversal of convergence direction and consistent interevent time lengths (Dragert *et al.* 2001; Miller *et al.* 2002; Obara *et al.* 2004; Szeliga *et al.* 2008).

Together, the results of our forward modelling and the suggestion of transient deformation both suggest that the Makran subduction zone is, at the minimum, coupled and accumulating strain throughout its length and therefore poses a significant seismic hazard to the regional population centres of southern Iran, Pakistan and Oman.

1.2 Palaeoseismic evidence of past megathrust seismicity

The hypothesis that the western Makran subduction zone is seismically quiescent compared to the eastern Makran stems largely from palaeoseismic studies conducted throughout the southern coast of Iran (Page *et al.* 1979; Shah-hosseini *et al.* 2011; Rajendran *et al.* 2013). In addition to these studies, Ambraseys & Melville (1982) have also compiled an extensive record of known historical earthquakes based on the sparse oral and written histories for the Makran. All of these studies conclude that there have been few large earthquakes along the western portion, in particular over the last 500 yr, and only one significant event, presumed to have occurred in 1483 with an inferred magnitude of M_w 8.0. However, Ambraseys & Melville (1982) indicate that available oral records for this event are few and they are unable to corroborate the location and date precisely. Similar circumstances hold for many other historic earthquakes in this region and even notable earthquakes could have gone unrecorded. Geomorphological investigations of coastal terraces, by contrast, indicate the western segment has undergone about 2 m of uplift in the Holocene, with possible tsunami wave heights of up to 4 m tentatively associated with an earthquake dated to 1008 AD (Ambraseys & Melville 1982; Shah-hosseini *et al.* 2011), but there is little direct palaeoseismic evidence to indicate that large earthquakes have occurred on the western half in the last ≈1000 yr. (Page *et al.* 1979; Shah-hosseini *et al.* 2011; Rajendran *et al.* 2013).

Along-strike segmentation could provide an explanation for the apparent differences in seismicity along the Makran (Byrne *et al.* 1992; Rajendran *et al.* 2013). Differences in seismicity have been seen along other margins where low plate coupling are seen (Ruff & Kanamori 1983; Savage *et al.* 1986; Pacheco *et al.* 1993; Reyners 1998; Métois *et al.* 2012). Furthermore, structures on the overriding Eurasian plate, such as the Sistan suture zone (Tirrul *et al.* 1983) as well as structures on the subducting Arabian plate, such as the Sonne fault (Kukowski *et al.* 2000) could provide a structural locus for such segmentation. Guided by the historical and palaeoseismic results, it has been hypothesized that the Makran may be segmented along-strike into two sections with fundamentally different interseismic coupling profiles (Byrne *et al.* 1992). While along-strike segmentation has been observed in other subduction zones (Fournier & Freymueller 2007; Métois *et al.* 2012), the evidence in these cases is primarily geodetic.

Estimates of the maximum magnitude for subduction zone earthquakes in the Makran have been less influenced by arguments for along-strike segmentation. Recently, Heidarzadeh *et al.* (2008) and Smith *et al.* (2013) calculated new estimates for moment magnitude for the Makran based on thermal studies and fault geometry and established an upper limit of about $M_w \approx 9.0$ based on the assumption that the entire margin is seismically coupled. These two studies largely ignore previously defined segment boundaries and focus on rupture lengths of full margin rupture, eastern half only rupture and central segment only rupture.

2 METHODS

2.1 Arabian–Eurasian plate interface geometry

In order to estimate fault coupling and strain accumulation in the Makran, a model for the geometry of the subducting Arabia plate interface is required. To our knowledge, no fault model for the Makran currently exists (Hayes *et al.* 2012). Since the data required to produce a high-resolution plate model do not exist for this region, we attempt to place bounds on the geometry of the plate by constructing three preliminary plate models for the Makran subduction zone. All of these plate models are constrained to meet the surface at the topographic expression of the trench as determined from GEBCO08 global ocean bathymetry. Our simplest and least realistic plate model, consists of a planar fault dipping at 15 deg, a value chosen from the average of the dips observed at shallow depths in the Slab 1.0 model (Hayes *et al.* 2012).

Our second model is based on a 3-D extrapolation of the profiles for east and west Makran from Byrne *et al.* (1992). These profiles were produced from a combination of diverse data sets including small-scale microearthquake analysis, earthquake slip vector analysis and petroleum reconnaissance geology. From these two profiles, a third profile, intermediate to the east and west profiles was created by simple averaging. These three profiles were then combined in three dimensions and contoured with an adjustable tension continuous curvature surface gridding algorithm (Fig. 1; Smith & Wessel 1990).

Our third model is based on a combination of our interpretation of available hypocentral locations from the International Seismological Centre (ISC) and moment tensors from the GlobalCMT (International Seismological Centre 2011; Ekström *et al.* 2012). To create this plate interface model, we utilize 61 yr of earthquake hypocentral data from the Reviewed ISC Bulletin, spanning 1950 January 1 to 2011 March 1; the extent of all reviewed seismic data for Pakistan and Iran (International Seismological Centre 2011). We project seismic hypocentres landward of the Makran trench along five evenly spaced profiles perpendicular to the trench (Figs 1 and 2). Earthquake hypocentres are binned in 100 km wide swaths along-strike to avoid overlap with adjacent trench-perpendicular profiles. Due to the lack of obvious Wadati–Benioff seismicity, coarse histograms, binned in 5 km depth increments and 50 km along-profile (strike perpendicular) increments were used to tentatively identify the separation between crustal and intraslab seismicity. For each transect, the points lying along this putative separation between crustal and intraslab seismicity were then connected to produce five smooth monotonically decreasing estimates of the plate interface. Where possible, focal mechanisms from the Global Centroid Moment Tensor project (Dziewonski *et al.* 1981; Ekström *et al.* 2012) were utilized to discern crustal from intraslab seismicity to constrain our plate geometry (Fig. 2). Thrust faulting mechanisms were assumed to occur along the plate interface at the upper boundary of the subducting oceanic lithosphere, while normal faulting mechanisms at depth were assumed to occur within the subducted oceanic lithosphere. The five profiles were then combined in three dimensions and contoured with an adjustable tension continuous curvature surface gridding algorithm (Smith & Wessel 1990).

Comparison between our second and third models shows overall agreement in the gross structure of the plate interface. Furthermore, the location of intraplate seismicity in the subducted Arabian plate suggests that our second model provides an upper bound for the top of the subducted and our model three provides a lower bound for the top of the subducted slab (Fig. 2). In addition, the resulting location of the volcanic arc relative to plate depth (55 km plate contour of model two, 85 km plate contour of model three) provides a check on the reasonableness of our method and suggests that our plate geometries are at least plausible. In all likelihood, the true plate interface lies at a depth between our model two and three plate interfaces. In the remainder of the paper, we will refer to model two as the shallow model and model three as the deep model. For subsequent strain accumulation modelling, we divide our plate interface surface into 81 rectangular polygons and calculate

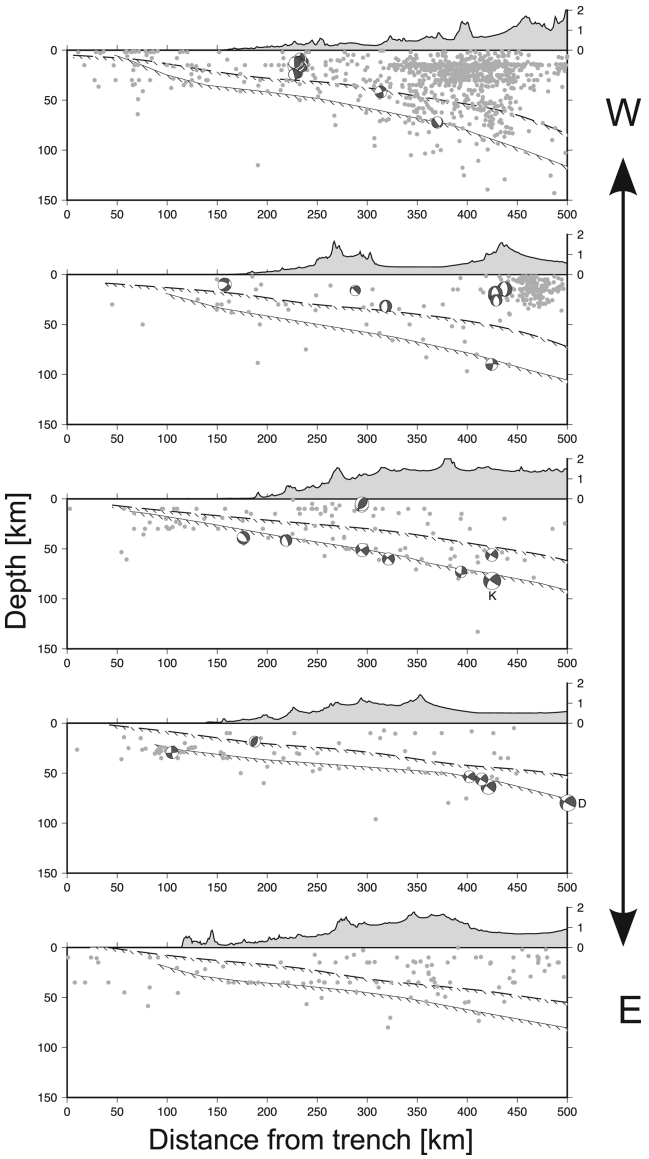

Figure 2. Cross-sections of seismicity showing the deep plate interface (solid line with hachures) and the shallow plate interface (dashed line with hachures). Both plate interfaces represent possibilities for the location of the top of the incoming Arabia plate. Grey dots are earthquake hypocentres from the revised ISC catalogue from the period 1950–2010 (International Seismological Centre 2011). Moment tensors are from the Global Moment Tensor catalogue (Ekström *et al.* 2012) and are shown in cross-section. These moment tensors have been plotting using depths from the revised ISC catalogue. Topography is shown with 20× exaggeration, while depth and distance from the trench are plotted 1-to-1. The surface expression of the trench identified from GEBCO08 global ocean bathymetry is located at 0. The 2011 Dalbadin earthquake and the 2013 Khash earthquakes are denoted by the letters D and K, respectively.

elastic Green's functions using the closed-form solutions provided by Okada (1992).

2.2 GPS measurements

Data from 20 GPS stations in southern Iran, southwestern Pakistan and northeastern Oman and 23 regional IGS stations were processed using the GAMIT analysis package (Herring *et al.* 2010a) of which 12 were used to assess interplate coupling. The remaining stations lie largely to the east of the subducting plate, where crustal strain rates related to continental dynamics processes eclipse the subduction-related interseismic deformation (Fig. 3). We use a baseline processing strategy combining daily GPS phase observations while holding IGS final orbits fixed to calculate loosely constrained estimates of station position and covariance using GAMIT version 10.50 (Herring *et al.* 2010a). These loosely constrained station position and covariance estimates were then used as input to GLOBK version 5.20 (Herring *et al.* 2010b) to estimate consistent station coordinates and velocities. Station coordinates and velocities are tied to a global reference frame through simultaneous processing of GPS phase data from 23 regional IGS stations. We realize our reference frame by minimizing the difference between published positions and velocities for ITRF2008 (Altamimi *et al.* 2011) and our results yielding a post-fit rms of 1.9 mm in position and 0.7 mm yr^{-1} in velocity. We then rotate our station velocities into a Eurasia-plate-fixed reference frame using the pole-of-rotation parameters published in Altamimi *et al.* (2012; Table 1). We account for correlated noise in our GPS time-series by using the 'real sigma' method of Herring (2003) and find a median random walk scaling of 0.147 $mm^2\ yr^{-1}$ in the north and 0.183 $mm^2\ yr^{-1}$ in the east.

3 MODELLING INTERSEISMIC DEFORMATION

Using the backslip method of Savage (1983) with elastic Green's functions computed for a homogeneous elastic half-space (Okada 1992) and the fault orientations from each of our plate models, we calculate interseismic deformation in the hangingwall of the Makran subduction zone. We constrain plate coupling to decrease linearly downdip to zero. Due to the location of the volcanic arc, we also make the assumption that below the 90 km contour, the subducting Arabian plate is definitely in contact with the mantle wedge and strain accumulation signals from fault elements deeper than 90 km are not recorded on the surface by GPS stations (Ruff & Kanamori 1983). To drive subduction we use the GEODVEL plate motions for Arabia relative to Eurasia (Argus *et al.* 2010) which are in better agreement with the velocities measured at GPS stations located on the subducting Arabian plate nearest to the trench in Oman (YIBL, MUSC, KHAS, Fig. 3) than longer term plate velocity values from reference frames such as NUVEL 1A (DeMets *et al.* 1994) or MORVEL (DeMets *et al.* 2010). Due to the proximity of the trench to the relative pole of rotation between Arabia and Eurasia (28.3N 28.9E; Argus *et al.* 2010) there exists a non-insignificant convergence rate difference of 21 per cent from west to east along the subducting margin. This west-to-east velocity increase is therefore taken in to account during forward modelling. In addition, the azimuth of convergence between the Arabian and Eurasian plates does not lie perpendicular to the strike of the trench (Fig. 1). To account for this, we assume that all motion oblique to convergence is accommodated on the subduction interface. While this results in a greatly improved fit to the observed velocity azimuths, it is likely that any oblique component is partitioned to some unknown degree between the subduction interface and faults in the overriding Eurasian plate. This idea is bolstered by the recent, complicated ruptures along the arcuate thrust faults of Baluchistan (Avouac *et al.* 2014). Due to the low signal-to-noise ratio of vertical GPS positions combined with our sparse spatial distribution of GPS observations, we consider only the horizontal shortening signal.

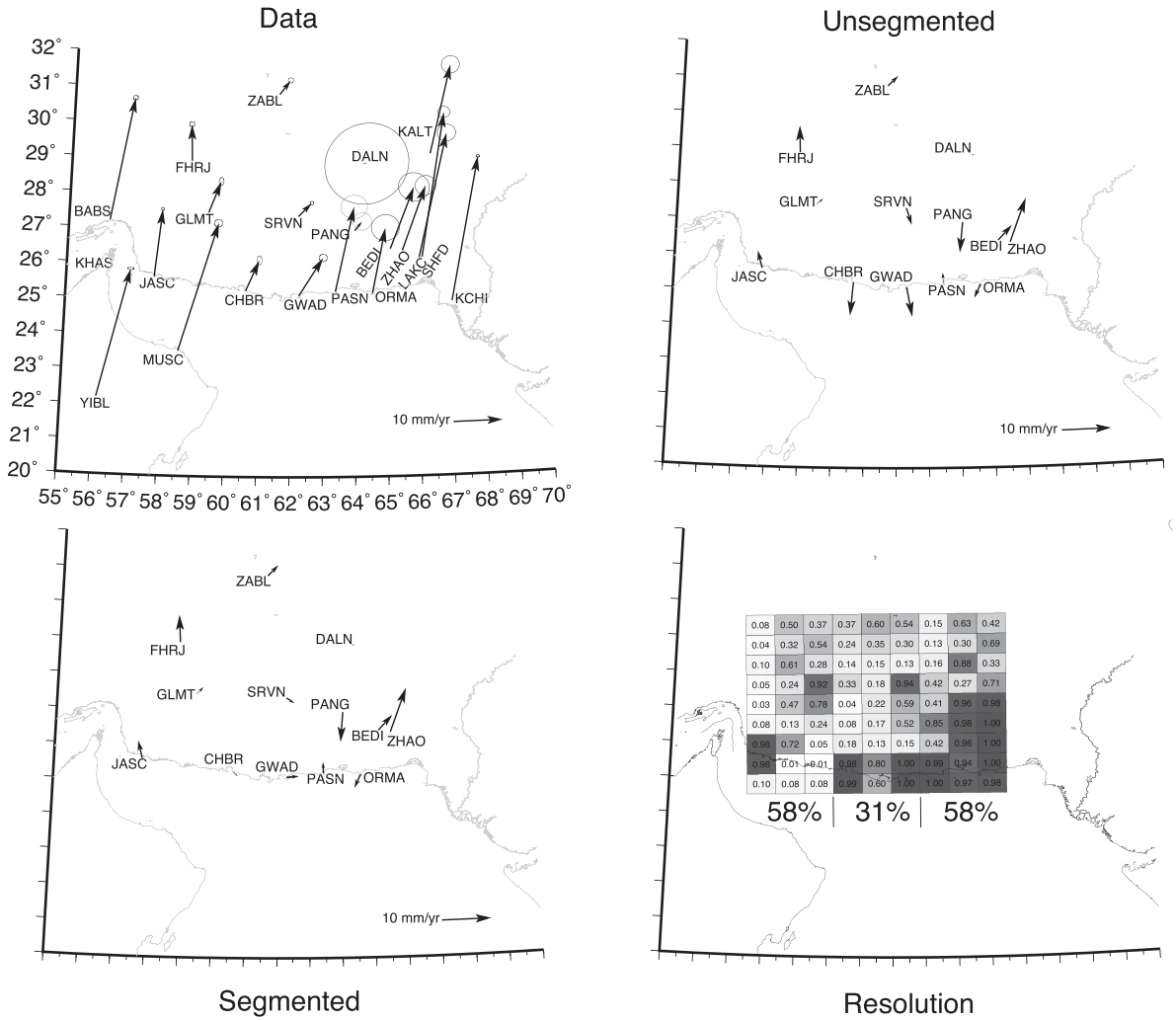

Figure 3. Velocities and residuals for segmented and unsegmented models and model resolution matrix. Velocities are relative to stable Eurasia and are all plotted at the same scale. Only GPS vectors that are directly influenced by subduction of the Arabia plate are shown in both the Segmented and Unsegmented residual velocity plots. The model resolution matrix (Resolution) is shaded and enumerated to show the percentage of slip recoverable on each fault element. In addition, the amount and extent of our best estimate of plate coupling for the segmented model is shown along the southern edge of the fault.

To identify the best-fitting models, we perform a grid search by uniformly varying both the coupling at the trench and the locking depth. We begin by choosing a coupling percentage at the trench relative to the expected GEODVEL rate (29.46 mm yr^{-1} at the western terminus of the trench) and a locking depth. Then, for each of our three fault geometries, we compute a forward model to predict the interseismic deformation rate using the methods outlined in Savage (1983) at the location of each GPS observation. We then compute the Akaike Information Criterion adjusted for small sample size from the sum of squared errors between each forward model and our observed horizontal GPS velocities using the formula,

$$\mathrm{AIC}_c = n \log\left(\frac{\sum(\frac{\epsilon}{\sigma})^2}{n}\right) + 2k + \frac{2k(k+1)}{n-k-1},$$

where n is the number of observations, k is the number of variable parameters and ϵ is the residual between data and model and σ is the associated uncertainty of each data point (Burnham & Anderson 2002). Once this grid search was completed for each of the three candidate plate models, model selection and comparison was accomplished using differences in the Akaike Information Criterion ($\Delta\mathrm{AIC}_c$) relative to the global minimum sum of squared errors (Burnham & Anderson 2002).

4 RESULTS

4.1 Without segmentation

Given the observed decrease in velocities (Fig. 3) as one moves towards the stable part of the Eurasian plate, the most basic observation that can be made from the processed GPS data in the Makran subduction zone is that the whole subduction zone is coupled to some degree. Thus, we begin by investigating the predicted locking pattern along the margin without considering segmentation. If we consider $\Delta\mathrm{AIC}_c$ values greater than 3 to indicate a low level of empirical support for a model (Burnham & Anderson 2002), we may identify broad boundaries on both the locking depth and coupling rate at the trench (Fig. 4). We find that both the deep plate model and the simple plane plate model perform poorly ($\Delta\mathrm{AIC}_c > 7$ denoting considerable loss of information) compared to the shallow plate interface developed in this paper. For the shallow model, the

Table 1. GPS velocities relative to the stable Eurasian plate as defined by Altamimi *et al.* (2012).

Longitude	Latitude	East (mm yr^{-1})	East uncertainty (mm yr^{-1})	North (mm yr^{-1})	North uncertainty (mm yr^{-1})	Correlation	Name
67.11287	24.93144	6.45	0.14	29.03	0.11	0.004	KCHI
66.60140	29.10583	4.78	0.75	17.87	0.72	0.018	KALT
66.22359	26.19502	5.42	0.50	29.16	0.47	0.012	LAKC
66.12940	26.18228	6.40	0.76	25.06	0.70	0.017	SHFD
65.60532	26.39270	5.10	0.86	13.04	0.80	0.035	ZHAO
65.22591	26.44925	5.12	1.28	12.37	1.18	−0.054	BEDI
64.63393	25.20879	2.89	1.16	13.16	1.08	0.014	ORMA
64.40259	28.88538	0.85	3.49	−0.15	3.36	0.066	DALN
64.10960	26.97782	1.56	0.78	1.85	0.73	0.033	PANG
63.46840	25.25882	4.01	1.11	17.14	0.97	0.024	PASN
62.32033	25.14408	4.99	0.34	7.69	0.31	0.036	GWAD
62.31832	27.39024	2.72	0.15	2.72	0.15	0.000	SRVN
61.71592	30.84128	2.25	0.23	2.87	0.22	0.008	ZABL
60.65113	25.28080	2.77	0.22	6.21	0.37	0.010	CHBR
59.44851	27.48216	2.48	0.20	6.39	0.32	0.002	GLMT
58.88126	28.93733	−0.22	0.22	7.40	0.20	−0.003	FHRJ
57.76989	25.63753	1.35	0.12	13.71	0.13	0.010	JASC
56.30785	27.20391	4.07	0.21	24.86	0.19	0.001	BABS
56.11234	22.18646	5.90	0.27	26.12	0.11	0.008	YIBL

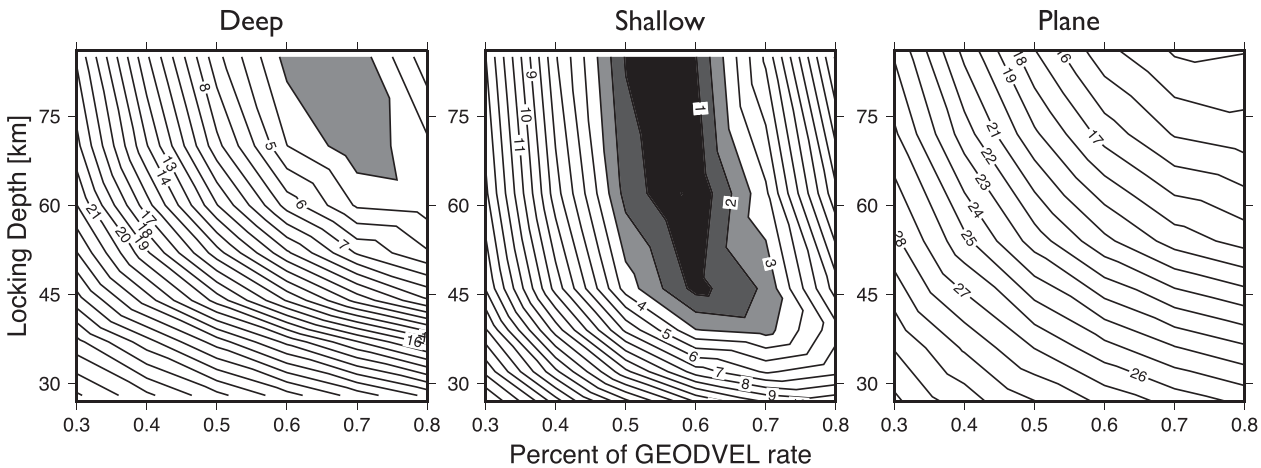

Figure 4. Contours of ΔAIC as a function of locking depth in km and percentage of GEODVEL rate (100 per cent = 29.46 mm yr^{-1} at the western terminus of the trench). Values of ΔAIC are calculated from the minimum AIC of all forward models, thus allowing model comparison and selection. From an information theoretic standpoint, ΔAIC can be interpreted to indicate the amount of empirical support a model has, with regions of ΔAIC < 3 suggesting substantial empirical support (Burnham & Anderson 2002). Thus, shading indicates the region of relative empirical support, with the darkest shading denoting the region where model parameters retains the most information.

values corresponding to $AIC_c < 3$ place bounds on plate coupling of between 46 and 72 per cent with locking depths as shallow as 38 km (Fig. 4, Shallow). It is possible to express the (mathematical) likelihood of a particular model given the observed data using these ΔAIC_c values. These likelihood values can then be used as weights (called Akaike weights in Burnham & Anderson 2002) to predict the values of locking depth and plate coupling corresponding to the best model in a Kullback–Liebler sense (Burnham & Anderson 2002). Using this approach, our Kullback–Liebler best model parameters for the shallow plate model correspond to a plate coupling of 58 per cent with a locking depth of 64 km. Our lack of sensitivity to the locking depth is entirely a function of GPS station distribution (Fig. 3) and should not be interpreted as evidence of anomalously deep locking on the Makran subduction zone.

4.2 With segmentation

The observed horizontal velocities along the central portion of the Makran coast near Gwadar, Pakistan (GWAD) and Chabahar, Iran (CHBR) and inland to Saravan, Iran (SRVN) are slower than those predicted by the best-fit models without segmentation by an average of 34 per cent (Fig. 3, Segmented). These slower velocities suggest that a further reduction in plate coupling is present along a central segment of the subduction zone as hypothesized by previous authors (Byrne *et al.* 1992; Rajendran *et al.* 2013). Beginning with our best unsegmented model, we perform a grid search over plate interface segment length and coupling reduction percentage. We then compute ΔAIC_c values in comparison with our best fit from our unsegmented model search. We find that there is considerable support ($\Delta AIC_c = 8.75$ improvement from the unsegmented model)

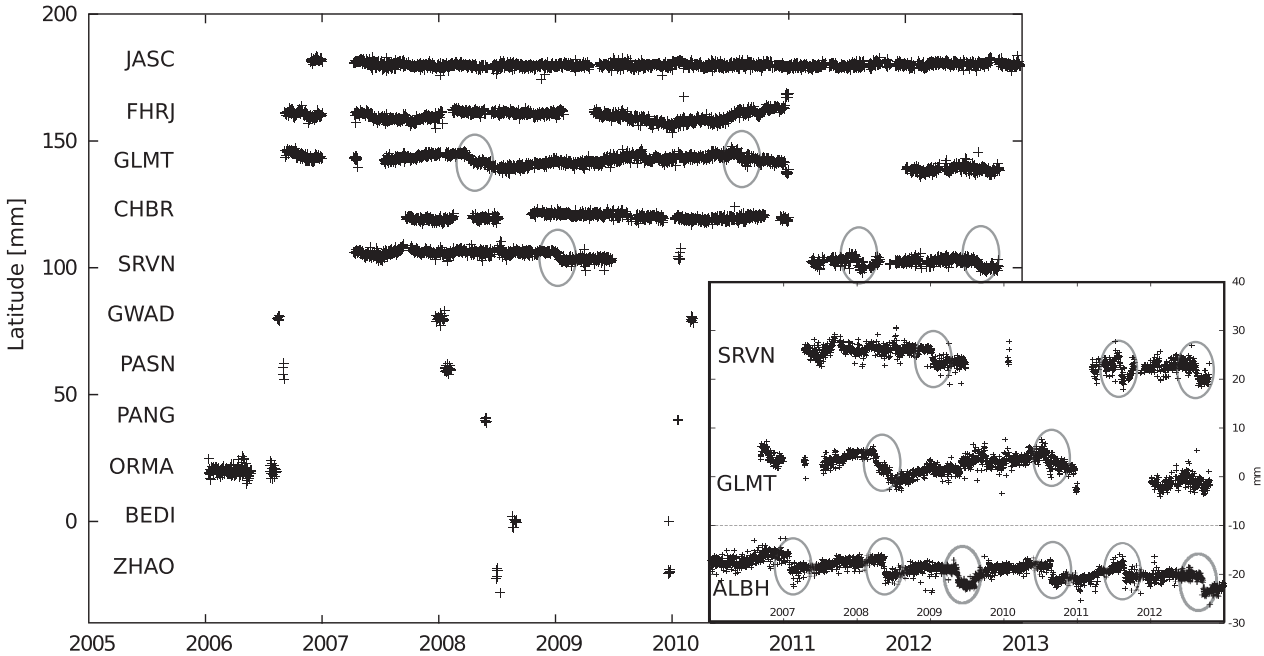

Figure 5. GPS time-series with secular velocities removed. North components are shown. Time-series are arranged by station location along the margin, with west at the top and east at the bottom. Possible slow-slip events at stations GLMT and SRVN are highlighted with ellipses. Inset shows the comparison between time-series behaviour during possible slow-slip events at stations SRVN and GLMT, with known slow-slip events from the Cascadia subduction zone recorded on the east component of station ALBH, in Albert Head, BC.

for a central segment of between 229 and 347 km with a plate coupling of 25–36 per cent centred near the Pakistan–Iran border. The Kullback–Leibler best model for segmentation corresponds with a 287 km low coupling zone with a plate coupling of 31 per cent (Fig. 3).

5 EVIDENCE FOR TRANSIENT SLOW SLIP

The processed GPS time-series suggest transient slow-slip events may also occur in the Makran subduction zone. Stations in Saravan, Iran (SRVN) and Golmorti, Iran (GLMT) show signals suggestive of transient deformation events like those seen geodetically in Cascadia (Dragert *et al.* 2001), Japan and a host of other subduction zones (Obara *et al.* 2004; Schwartz & Rokosky 2007; Kimura *et al.* 2011; Fig. 5). Time-series for both these stations show transient displacements of 4.6 mm displacement to the south at SRVN and an average displacement of 3.5 mm to the south at GLMT. The dominantly southward direction of deformation is consistent with slip along the Arabian–Eurasian plate interface, which is accommodating nearly north–south convergence in this region. The observed transient deformation events also appear to last about 15 d in duration, again similar to slow-slip durations seen in Cascadia, Costa Rica and elsewhere (Rogers & Dragert 2003; Schwartz & Rokosky 2007; Szeliga *et al.* 2008; Outerbridge *et al.* 2010; Dragert & Wang 2011). There are, however, no GPS stations in the forearc basin proper, and we only see four possible transient deformation events recorded on these two stations. Lacking the necessary station density in the forearc, we cannot conclusively prove that slow-slip-like events occur in the Makran. However, the many similarities between these observations and subduction zone slow-slip events recognized elsewhere in the world suggest they are likely due to slow-slip-related transient deformation rather than other sources, for instance, monument instability. In future work, geodetic instrument densification could allow slow slip to be used to estimate the downdip extent of interseismic coupling, as has been done elsewhere (Chapman & Melbourne 2009).

6 DISCUSSION

While the shallow plate interface model is our preferred plate model based on its fit to the GPS constrained horizontal shortening rate (Fig. 4), other features, notably the location of the volcanic arc, also provide constraints. Global analysis of subducted plate depths beneath volcanic arcs shows an average depth of 105 km with a range of 72–173 km (England *et al.* 2004; Syracuse & Abers 2006). However, the depth to the top of the subducting slab beneath the volcanoes of the Makran is only 55 km in the shallow model. This seems unreasonably shallow and would make the volcanoes of the Makran some of the shallowest volcanoes on Earth, relative to their subducted slab: shallower than either the eastern Aleutian arc, whose volcanoes are, on average, 65 ± 5 km above the plate interface (England *et al.* 2004) or the Ryukyu arc whose volcanos average 71.5 ± 23.0 km (Syracuse & Abers 2006). On the other hand, our deep model places the volcanoes above the 85 km depth contour, which, while still shallow in comparison to most volcanic arcs, is not unusually so. Additionally, the 2011 Dalbadin and 2013 Khash earthquakes, both intraslab events, also provide a check on slab depth (Fig. 2). These events are thought to have ruptured significant thicknesses of the subducted Arabian Plate (Barnhart *et al.* 2014). Therefore, our deep model is constrained to be no deeper than the origin of these earthquakes, and, in a similar way, our shallow model is constrained to be no shallower than a reasonable slab thickness above these origins. It is likely that the true plate interface consists of a combination of the shallow portion of the shallow plate interface model (to satisfy our GPS observations) and the deep portion of our deep plate interface model (to satisfy our volcanic arc and intraplate seismicity requirements).

Another complication in creating a realistic and useful plate model for the Makran is delineating the extent of the subducted plate. Delineation of the edges of the subducted Arabian plate using the surface velocity field, in particular, the eastern edge, is complicated because of the nearly identical motion of both Arabia and India relative to Eurasia. Indeed, inspection of the velocities relative to stable Eurasia of stations along the eastern edge of the Makran all show similar lengths and azimuths (compare Karachi, Pakistan (KCHI) with Yibal, Oman (YIBL); Fig. 3). Surface geology and neotectonics are also of no help, as the actual location of the plate boundary between India and Eurasia along the southernmost extent is not clearly defined by obvious surface faulting either (Szeliga *et al.* 2012). The most straightforward option is to use the extent of the bathymetric expression of the trench as our guide in determining the plate edge. Thus, we have chosen as our slab edge, a line running from the eastern end of the bathymetric expression of the trench and perpendicular to the strike of the trench. This scheme effectively assigns GPS sites, such as LAKC, SHFD and ZHAO to the Indian plate and BEDI to the Eurasian plate as in Szeliga *et al.* (2012) (Fig. 1). Even with this arrangement, it is clear that a simple elastic model fails to account for the observed station motion in this complex deforming region (Fig. 3). Identification of the western edge of the plate is more straightforward thanks to the surface expression of the Minab–Palami fault system (Yamini-Fard *et al.* 2007; Ul-Hadi *et al.* 2013) and the similar velocities at Khasab, Oman (KHAB) and Bandar Abbas, Iran (BABS). In fact, the velocity and direction of secular motion at BABS suggest that this station is more strongly coupled to the Arabian plate than the Eurasian plate, on which it appears to reside (Fig. 3).

While our GPS observations from the Makran are sparse, our model resolution matrix (Fig. 3) indicates that our ability to resolve slip along the majority of the coast of the margin is good (resolution > 0.9) (Menke 1989). Further to the north, our network thins considerably and our model resolution becomes much worse. Thus, our most robust prediction of plate coupling occurs closest to the trench. Unfortunately, the spatial distribution of stations is not optimal to provide precise limits on the downdip locking depth (Fig. 3). However, our coastal observations provide some constraints and are consistent with a locking depth no shallower than 38 km. This locking depth is consistent with observations in other subduction zones (Ruff & Kanamori 1983).

From a plate coupling standpoint, our preferred model essentially segments the Makran subduction zone into three regions (Fig. 3). The easternmost region, from approximately midway between Gwadar, Pakistan and Pasni, Pakistan (GWAD and PASN; Figs 1 and 3) to the eastern end of the trench appears to be coupled at about 58 per cent. This is the region with the highest rates of historical seismicity as well as the only segment with a documented megathrust event (Byrne *et al.* 1992). The central region of the three regions spans the coast from just east of Gwadar, Pakistan to a point just west of Chabahar, Iran (GWAD and CHBR; Figs 1 and 3). This region appears to show a reduction in plate coupling from 58 per cent to 31 per cent. This low plate coupling is similar to that found in the Shumagin Islands, Alaska (Fournier & Freymueller 2007). However, unlike the Shumagin Islands which have experienced major earthquakes in the past century, there is no evidence for historical rupture along the central Makran. Finally, the westernmost region, which encompasses the margin from west of Chabahar Bay to the entrance to the Straits of Hormuz west of Bandar-e-Jask, Iran (JASC; Fig. 1) is the most poorly resolved and appears to be best fit by a plate coupling larger than the central region, and possibly similar to that of the easternmost region. The primary constraint on increased plate coupling in the westernmost segment is the increased velocity observed at JASC (Fig. 3). This increased velocity also provides a constraint on the maximum width of the low plate coupling region. However, the low station coverage in this region does not allow us to determine the precise extent.

Our division of the Makran margin into segments has implications for the maximum magnitude of earthquakes along the margin. Determining the maximum magnitude depends on what is meant by plate coupling and what its relationship is to future seismicity. If we equate plate coupling to seismic coupling, we may follow the model of Ruff & Kanamori (1983), which suggests that plate coupling is an predictor of average asperity size. In this case, low plate coupling would indicate the presence of many small seismic asperities per unit of trench length. This would imply that typical earthquakes along the central segment should have a lower magnitude than typical earthquakes along the eastern (and possibly western) segment. However, even if this distribution of asperity sizes were true, it is still unknown whether rupture could continue across a segment boundary thus producing a much larger earthquake than the simplest view the asperity model could suggest. Thus, two possibilities present themselves, single segment rupture and multi-segment rupture. Using our plate coupling segment dimensions for the Makran, we have three segments with along-strike lengths of roughly 300 km each. Since earthquake magnitude, fault area and average fault slip are all related through the stress drop, and since stress drop appears constant as a function of earthquake magnitude (Kanamori & Anderson 1975), we may use our knowledge of fault area and reasonable upper limits for stress drop to approximate the upper limits for earthquake magnitude. Thus, assuming a stress drop of 10 MPa during a large megathrust event, each one of these segments could be capable of an M_w 8.4 (eq. (4.20), Stein & Wysession 2003, 38 km downdip width, 275 km along-strike length). Conveniently, this magnitude is similar to some estimates of the magnitude for the 1945 Makran earthquake (Geller & Kanamori 1977; Page *et al.* 1979; Quittmeyer 1979; Byrne *et al.* 1992), which occurred in what we have called the easternmost segment. On the other hand, if a change in asperity size in the central segment presents no barrier to rupture, a 10 MPa stress drop would yield an upper magnitude of M_w 8.8 for a margin-wide megathrust earthquake (38 km downdip width, 900 km along-strike length).

It is also possible that plate coupling is a manifestation of partitioning between interplate slip and shortening in the overriding plate (Nicol & Beavan 2003). In this system, regions of low plate coupling would correspond with a decrease in magnitude of folding in the overriding plate. In some subduction systems, this equates to backarc extension, a feature not seen in the Makran. Thus, if we were to equate plate coupling to a larger scale slip partitioning between interplate slip and intraplate shortening, we would need estimates of longer term (geological) shortening rates in the overriding plate.

A third possibility is that plate coupling can be modulated by the presence of overpressurized fluids in both the hangingwall and along the plate interface. Modelling of the effects of fluid pressure on plate coupling by Fagereng & Ellis (2009) suggest that fluid overpressure in both the hangingwall and along the plate interface results in increased plate coupling, while hydrostatic fluid pressures would result in lower plate coupling. The most obvious indication that fluids in the hangingwall are overpressurized in the Makran is the presence of mud volcanoes along the coast (e.g. Delisle *et al.* 2002). While the majority of the active mud volcanoes in the Makran are in the easternmost segment, mud volcanism extends nearly the entire length of the margin (Snead 1964; Wiedicke *et al.* 2001;

Delisle 2004). Thus, the precise role that fluid pressures play in modulating plate coupling in the Makran is likely complicated at best.

7 CONCLUSIONS

The Makran subduction zone is partially locked, and accumulating strain at a rate of between $17.1^{+4.1}_{-3.5}$ mm yr^{-1}. This corresponds to a plate coupling ratio of 58 per cent (46–72 per cent) between the subducting Arabian Plate and the overriding Eurasian Plate. In addition to the overall low plate coupling, we find evidence for a channel of lower plate coupling (31 per cent) along the central-western portion of the Makran. The lower plate coupling ratios seen here are similar to those found near the Sanak Islands and the Shumigan Gap in the Aleutians. Locking depths in the Makran are poorly constrained due to the low station density, with an updip limit possibly as shallow as 38 km.

ACKNOWLEDGEMENTS

We would like to thank Sarosh Hashmat Lodi and Amir Abolghasem for gathering the GPS data and processing of data. EF was supported by NASA ROSES grant #NNXlOAD15G. We thank Generic Mapping Tools (GMT) for production of maps. Ocean bathymetry was obtained from The GEBCO_08 Grid, version 20100927, http://www.gebco.net. In addition, this manuscript benefitted greatly from reviews by Rob McCaffrey and Rebecca Bendick.

REFERENCES

Altamimi, Z., Collilieux, X. & Métivier, L., 2011. ITRF2008: an improved solution of the international terrestrial reference frame, *J. Geod.,* **85,** 457–473.

Altamimi, Z., Métivier, L. & Collilieux, X., 2012. ITRF2008 plate motion model, *J. geophys. Res.,* **117,** doi:10.1029/2011JB008930.

Ambraseys, N. & Melville, C.P., 1982. *A History of Persian Earthquakes,* Cambridge Univ. Press.

Argus, D., Gordon, R.G., Heflin, M.B., Ma, C., Eanes, R.J., Willis, P., Peltier, W.R. & Owen, S., 2010. The angular velocities of the plates and the velocity of Earth's centre from space geodesy, *Geophys. J. Int.,* **180,** 913–960.

Avouac, J. *et al.*, 2014. The 2013, M_w 7.7 Balochistan earthquake, energetic strike-slip reactivation of a thrust fault, *Earth planet. Sci. Lett.,* **291,** 128–134.

Barnhart, W., Hayes, G., Samsonov, S., Fielding, E. & Seidman, L., 2014. Breaking the oceanic lithosphere in subduction zones: the 2013 Khash, Iran earthquake, *Geophys. Res. Lett.,* **41,** 32–36.

Burnham, K.P. & Anderson, D.R., 2002. *Model Selection and Multimodal Inference: A Practical Information-theoretic Approach,* 2nd edn, Springer-Verlag.

Byrne, D.E., Sykes, L.R. & Davis, D.M., 1992. Great thrust earthquakes and aseismic slip along the plate boundary of the Makran subduction zone, *J. geophys. Res.,* **97**(1), 449–478.

Chapman, J.S. & Melbourne, T.I., 2009. Future Cascadia megathrust rupture delineated by episodic tremor and slip, *Geophys. Res. Lett.,* **36,** doi:10.1029/2009GL040465.

Delisle, G., 2004. Mud volcanoes of Pakistan, *Environ. Geol.,* **46,** 1024–1029.

Delisle, G., von Rad, U., Andruleit, H., von Daniels, C.H., Tabrez, A.B. & Inam, A., 2002. Active mud volcanoes on- and offshore eastern Makran, Pakistan, *Int. J. Earth Sci.,* **91,** 93–110.

DeMets, C., Gordon, R.G., Argus, D. & Stein, S., 1990. Current plate motions, *Geophys. J. Int.,* **101,** 425–478.

DeMets, C., Gordon, R.G., Argus, D. & Stein, S., 1994. Effect of recent revisions to the geomagnetic reversal time scale on estimates of current plate motions, *Geophys. Res. Lett.,* **21**(20), 2191–2194.

DeMets, C., Gordon, R.G. & Argus, D., 2010. Geologically current plate motions, *Geophys. J. Int.,* **181,** 1–80.

Douglas, A., Beavan, J., Wallace, L. & Townend, J., 2005. Slow slip on the northern Hikuangi subduction interface, New Zealand, *Geophys. Res. Lett.,* **32,** doi:10.1029/2005GL023607.

Dragert, H. & Wang, K., 2011. Temporal evolution of an episodic tremor and slip event along the northern Cascadia margin, *J. geophys. Res.,* **116,** doi:10.1029/2011JB008609.

Dragert, H., Wang, K. & James, T.S., 2001. A silent slip event on the deeper Cascadia subduction interface, *Science,* **292,** 1525–1528.

Dziewonski, A.M., Chou, T.-A. & Woodhouse, J.H., 1981. Determination of earthquake source parameters from waveform data for studies of global and regional seismicity, *J. geophys. Res.,* **86**(4), 2825–2852.

Ekström, G., Nettles, M. & Dziewonski, A.M., 2012. The global CMT project 2004–2010: centroid-moment tensors for 13,017 earthquakes, *Phys. Earth planet. Inter.,* **200–201,** 1–9.

England, P., Engdahl, R. & Thatcher, W., 2004. Systematic variation in the depths of slabs beneath arc volcanoes, *Geophys. J. Int.,* **156,** 377–408.

Fagereng, A. & Ellis, S., 2009. On factors controlling the depth of interseismic coupling on the Hikurangi subduction interface, New Zealand, *Earth planet. Sci. Lett.,* **278,** 120–130.

Fournier, T.J. & Freymueller, J.T., 2007. Transition from locked to creeping subduction in the Shumagin region, Alaska, *Geophys. Res. Lett.,* **34**(6), doi:10.1029/2006GL029073.

Geller, R. & Kanamori, H., 1977. Magnitudes of great shallow earthquakes from 1904 to 1952, *Bull. seism. Soc. Am.,* **67,** 587–598.

Gomberg, J. & Cascadia 2007 and Beyond Working Group, 2010. Slow-slip phenomena in Cascadia from 2007 and beyond: a review, *Geol. Soc. Am. Bull.,* **122**(7–8), 963–978.

Hayes, G.P., Wald, D.J. & Johnson, R.L., 2012. Slab1.0: a three-dimensional model of global subduction zone geometries, *J. geophys. Res.,* **117,** doi:10.1029/2011JB008524.

Heidarzadeh, M., Pirooz, M.D., Zaker, N.H. & Synolakis, C.E., 2008. Evaluating tsunami hazard in the northwest Indian Ocean, *Pure appl. Geophys.,* **165,** 2045–2058.

Herring, T.A., 2003. MATLAB tools for viewing GPS velocities and time series, *GPS Solut.,* **7,** 194–199.

Herring, T.A., King, R.W. & McClusky, S.C., 2010a. GAMIT reference manual, GPS analysis at MIT release 10.4. Tech. Rep., Dept. Earth Atmos. Planet. Sci. Mass. Inst. Technol., Cambridge, MA.

Herring, T.A., King, R.W. & McClusky, S.C., 2010b. GLOBK: Global Kalman filter VLBI and GPS analysis program, release 10.4. Tech. Rep., Dept. Earth Atmos. Planet. Sci. Mass. Inst. Technol., Cambridge, MA.

International Seismological Centre, 2011. *On-line Bulletin,* Int. Seis. Cent., Thatcham, United Kingdom, http://www.isc.ac.uk, last accessed 22 May 2014.

Kanamori, H. & Anderson, D.L., 1975. Theoretical basis of some empirical relations in seismology, *Bull. seism. Soc. Am.,* **65**(5), 1073–1095.

Kimura, T., Obara, K., Kimura, H. & Hirose, H., 2011. Automated detection of slow slip events within the Nankai subduction zone, *Geophys. Res. Lett.,* **38**(1), doi:10.1029/2010GL045899.

Kopp, C. J. F., Flueh, E.R., Reichert, C., Kukowski, N., Bialas, J. & Klaeschen, D., 2000. Structure of the Makran subduction zone from wide-angle and reflection seismic data, *Tectonophysics,* **329,** 171–191.

Kukowski, N., Schillhorn, T., Flueh, E. & Huhn, K., 2000. Newly identified strike-slip plate boundary in the northeastern Arabian Sea, *Geology,* **28**(4), 355–358.

Menke, W., 1989. *Geophysical Data Analysis: Discrete Inverse Theory,* Academic Press.

Métois, M., Socquet, A. & Vigny, C., 2012. Interseismic coupling, segmentation and mechanical behavior of the Central Chile subduction zone, *J. geophys. Res.,* **117**(B3), doi:10.1029/2011JB008736.

Miller, M., Melbourne, T., Johnson, D. & Sumner, W.Q., 2002. Periodic slow earthquakes from the Cascadia subduction zone, *Science,* **295,** 2423, doi:10.1126/science.1071193.

Nicol, A. & Beavan, J., 2003. Shortening of an overriding plate and its implications for slip on a subduction thrust, central Hikurangi Margin, New Zealand, *Tectonics,* **22**(6), doi:10.1029/2003TC001521.

Obara, K., 2011. Characteristics and interactions between non-volcanic tremor and related slow earthquakes in the Nankai subduction zone, southwest Japan, *J. Geodyn.,* **52**(3), 229–248.

Obara, K., Hirose, H., Yamamizu, F. & Kasahara, K., 2004. Episodic slow slip events accompanied by non-volcanic tremors in southwest Japan subduction zone, *Geophys. Res. Lett.,* **31,** doi:10.1016/j.jog.2011.04.002.

Okada, Y., 1992. Internal deformation due to shear and tensile faults in a half-space, *Bull. seism. Soc. Am.,* **82**(2), 1018–1040.

Outerbridge, K.C. *et al.*, 2010. A tremor and slip event on the Cocos-Caribbean subduction zone as measured by a global positioning system (GPS) and seismic network on the Nicoya Peninsula, Costa Rica, *J. geophys. Res.,* **115,** doi:10.1029/2009JB006845.

Pacheco, J.F., Sykes, L.R. & Scholz, C.H., 1993. Nature of seismic coupling along simple plate boundaries of the subduction type, *J. geophys. Res.,* **98**(8), 14 133–14 159.

Page, W.D., Alt, J.N., Clufff, L.S. & Plafker, G., 1979. Evidence for the recurrence of large-magnitude earthquakes along the Makran coast of Pakistan, *Tectonophysics,* **52,** 533–547.

Quittmeyer, R., 1979. Seismicity variations in the Makran region of Pakistan and Iran: relation to great earthquakes, *Pure appl. Geophys.,* **117,** 1212–1228.

Rajendran, C.P., Rajendran, K. M., Shah-hosseini, M., Beni, A.N., Nautiyal, C.M. & Andrews, R., 2013. The hazard potential of the western segment of the Makran subduction zone, northern Arabian Sea, *Earth Environ. Sci.,* **65**(1), 219–239.

Reyners, M., 1998. Plate coupling and the hazard of large subduction thrust earthquakes at the Hikurangi subduction zone, New Zealand, *N.Z. J. Geol. Geophys.,* **41**(4), 343–354.

Rogers, G. & Dragert, H., 2003. Episodic tremor and slip on the Cascadia subduction zone: the chatter of silent slip, *Science,* **300,** 1942–1943.

Ruff, L. & Kanamori, H., 1983. Seismic coupling and uncoupling at subduction zones, *Tectonophysics,* **99,** 99–117.

Savage, J.C., 1983. A dislocation model of strain accumulation and release at a subduction zone, *J. geophys. Res.,* **88**(6), 4984–4996.

Savage, J.C., Lisowski, M. & Prescott, W.H., 1986. Strain accumulation in the Shumagin and Yakataga Seismic Gaps, Alaska, *Science,* **231,** 585–587.

Schwartz, S. & Rokosky, J.M., 2007. Slow slip events and seismic tremor at circum-Pacific subduction zones, *Rev. Geophys.,* **45,** doi:10.1029/2006RG000208.

Shah-hosseini, M., Morhange, C., Beni, A.N., Marriner, N., Lahijani, H., Hamzeh, M. & Sabatier, F., 2011. Coastal boulders as evidence for high-energy waves on the Iranian coast of Makran, *Mar. Geol.,* **290**(1–4), 17–28.

Smith, W.H.F. & Wessel, P., 1990. Gridding with continuous curvature splines in tension, *Geophysics,* **55,** 293–305.

Smith, G., McNeill, L., Henstock, T.J. & Bull, J., 2012. The structure and fault activity of the Makran accretionary prism, *J. geophys. Res.,* **117,** doi:10.1029/JB009312.

Smith, G., McNeill, L., Wang, K., He, J. & Henstock, T.J., 2013. Thermal structure and megathrust seismogenic potential of the Makran subduction zone, *Geophys. Res. Lett.,* **40**(8), 1528–1533.

Snead, R.E., 1964. Active mud volcanoes of Baluchistan, west Pakistan, *Geogr. Rev.,* **54**(4), 546–560.

Stein, S. & Wysession, M., 2003. *An Introduction to Seismology, Earthquakes, and Earth Structure,* Blackwell Scientific Publishers.

Syracuse, E.M. & Abers, G.A., 2006. Global compilation of variations in slab depth beneath arc volcanoes and implications, *Geochem. Geophys. Geosyst.,* **7**(5), doi:10.1029/2005GC001045.

Szeliga, W., Melbourne, T., Santillan, V.M. & Miller, M., 2008. GPS constraints on 34 slow slip events within the Cascadia subduction zone, 1997–2005, *J. geophys. Res.,* **113,** doi:10.1029/2007JB004948.

Szeliga, W., Bilham, R., Kakar, D.M. & Lodi, S.H., 2012. Interseismic strain accumulation along the western boundary of the indian subcontinent, *J. geophys. Res.,* **117,** doi:10.1029/2011JB008822.

Tirrul, R., Bell, I.R., Griffis, R.J. & Camp, V.E., 1983. The Sistan suture zone of eastern Iran, *Geol. soc. Am. Bull.,* **94**(1), 134–150.

Ul-Hadi, S., Khan, S.D., Owen, L.A., Khan, A.S., Hedrick, K.A. & Caffee, M.W., 2013. Slip-rates along the Chaman fault: implication for transient strain accumulation and strain partitioning along the western Indian plate margin, *Tectonophysics,* **608,** 389–400.

Wiedicke, M., Neben, S. & Spiess, V., 2001. Mud volcanoes at the front of the Makran accretionary complex, Pakistan, *Mar. Geol.,* **172,** 57–73.

Yamini-Fard, F., Hatzfeld, D., Farahbod, A.M., Paul, A. & Mokhtari, M., 2007. The diffuse transition between the Zagros continental collision and the Makran oceanic subduction (Iran): microearthquake seismicity and crustal structure, *Geophys. J. Int.,* **170,** 182–194.